JAST, Vol. 8, No. 2, pp 97–105

JAST
Journal of Aerospace Science and Technology

An Experimental Study of a Compound Control Method around a Cylinder

S. Reza-zadeh[1], H. Masumi[2] and E. Esmaeilzadeh[3]

In this research work, a compound flow control method (passive and active) has been described. EHD actuators as wire-plate (active) and a splitter plate (passive) were applied simultaneously to control the fluid flow and heat transfer around a circular cylinder. The investigation consists of the interaction between electric field, fluid flow and temperature field. Experimental tests included various positions of the splitter plate and two Reynolds numbers, Re=3500, 7000. EHD actuators were wire-plate electrodes. The cylinder and the splitter plate were connected to the ground and used as cathode electrodes. Pressure and temperature distributions over the surface of the cylinder were measured. The results show that two effective corona winds appear in the flow around the cylinder. The first corona wind is between wires and the cylinder and the second one is between wires and the splitter plate. The two corona winds affected the fluid flow and heat transfer. The presence of the splitter plate caused a decrease in drag force and an increase in heat transfer. By increasing gap distance, the effect of the second corona was reduced.

NOMENCLATURE

A_S	Cylinder surface (m^2)
$C_p = \frac{2(P-P_0)}{\rho U_0^2}$	Pressure coefficient
$C_d = \frac{2D_P}{\rho U_0^2 A_S}$	Drag coefficient
d	Diameter of cylinder (m)
D_p	Pressure drag force (N)
EHD	Electrohydrodynamic
G	Gap distance
H	Distance between the wire electrode and the cylinder
h	Coefficient of convection heat transfer
k	Coefficient of conductive heat transfer
L	Length of cylinder (m)
$Nu = \frac{hd}{k}$	Nusselt number
Nu_0	Nu number for leading edge of cylinder without control method
Nu_{ave}	Average Nu number over the cylinder surface
P	Pressure (N/m^2)
P_0	Surrounding pressure (N/m^2)
R	Radius of cylinder (m)
Re	Reynolds number based on diameter
U_0	Speed of mainstream (m/s)

Greek symbols

α	Angle of wire electrodes form leading edge in clockwise direction
θ	Angle over the cylinder from leading edge in clockwise direction
ρ	Density of the fluid
Δt	Time step(s)

INTRODUCTION

The fluid flow around a cylinder, because of some complicated phenomena such as vortex shedding and flow separation behind the cylinder, has been studied

1. *Assistant Prof., Dep't. of Mech. Eng., Hakim Sabzevari University, Iran, Email:s.rezazadeh@hsu.ac.ir*
2. *MSc. Student, Dept. of Mech. Eng., University of Tabriz, Tabriz, Iran*
3. *Professor, Dep't. of Mech. Eng., University of Tabriz, Tabriz, Iran*

by many researchers and scientists. They applied some methods and devices to control this flow. Most of these techniques change the boundary layer and the wake zone to obtain the best efficiency.

The methods are classified into three groups: (1) passive control, (2) active control and (3) compound control. The passive control techniques do not need any external energy during application. Additional devices in the fluid flow or changing the geometry of the bluff body such as splitter plate, base bleed and roughness are utilized in this method. The active control techniques such as EHD actuators and vibrators need external energy to affect the fluid flow. When the active and passive techniques are applied simultaneously, it is called compound method.

The splitter plate, as a passive method, is widely used for flow control. Using a circular cylinder with a connected splitter plate was reported by Roshko (1954). Then, others used it in different cases (Bearman, 1965; Aplet, 1973, 1975; Unal, 1978; Arai, 1992; Lin, 1994; Kwon, 1996; Boiaubert, 1998). Ozono (1999), (2000) performed some experiments by the splitter plate and the second cylinder in the wake zone. His experiments included different lengths and asymmetrically arranged splitter plate. He used detached a splitter plate at different gap distances. It was found that when the splitter was arranged asymmetrically, vortex shedding was critically suppressed and there was an ideal gap distance. Hwang *et.al.* (2003), (2007) considered the fluid flow in which the splitter plate was placed at various locations downstream of the cylinder. They found out the splitter plate significantly reduced drag force and lift fluctuation and there was an ideal location of the splitter for the maximum reduction. Tiwari *et.al.* (2005) investigated heat transfer around the cylinder with the splitter plate. They referred to a reduction in the size of the wake zone. The splitter plate was an extra fin area for conduction, so heat transfer increased. Shukla *et.al.* (2009) studied the fluid flow around the cylinder with a hinged-splitter plate in the wake zone. Their experiments showed that the splitter plate oscillation increases with Reynolds number at low Reynolds numbers.

Application of electrohydrodynamic (EHD) actuators was reported some decades ago. EHD is the interaction of electric and flow fields. High field strength around a sharp emitter produces ions and accelerates ions to opposite electrode. Energy transfer between charges and fluid molecules leads to flow motion which is called ionic wind or corona wind.

The corona wind was reported by Hauksbee (1719); then, others (Chattok, 1899; Steutzer, 1959; Robinson, 1961; Velkoff, 1968; Yabe, 1978; Rosendal, 1988; Crowly, 1990; Semoto, 1992; Ohadi, 1991; Seyed-Yaghoobi, 1991, 1992, 1995, 2003) used this phenomenon for various applications and developed it. Leger *et.al.* (2001), (2002) could reduce the wake zone behind a plate by EHD actuators and found out the kinetic energy induced by the ionic wind inside the boundary layer allows a drag reduction for low Reynolds numbers. Artana *et.al.* (2003) explored the fluid flow around a cylinder by wire-plate electrodes and adjusted the size of mean recirculation region behind the cylinder. Hyun *et.al.* (2003) performed some experiments to examine the effect of distance between electrodes. They found out the pressure drag can be affected by imposing corona wind. Onset of EHD turbulence was reported by Chang *et.al.* (2006) in the cross flow around a cylinder. They produced EHD turbulence even at low Reynolds numbers. Jukes *et.al.* (2009) used a dielectric barrier discharge (DBD) plasma actuator to control the flow around a cylinder.

In the present study, the compound method (passive and active) is introduced to control heat transfer and hydrodynamic around a cylinder. In this approach, a splitter plate, as a passive technique, and EHD actuators (wire-plate), as an active technique, are used simultaneously. The cylinder and the splitter plate are connected to the ground and used as cathode electrodes for EHD actuation. Experiments were performed to study various locations of the splitter plate G =0, 0.5d, d, 2d, α= $\pm 90^{\circ}$, H=R and Re=3500, 7000. Pressure and temperature are measured to study hydrodynamic and heat transfer in various cases.

Theory

EHD mechanisms can create motions in fluid that are single phase or multiphase flows. This motion forms a secondary flow in fluids. The electric force that is responsible for this motion is:

$$\vec{F} = \rho_e E - \frac{1}{2}E^2\nabla\epsilon + \frac{1}{2}\nabla\left[E^2\rho(\frac{\partial\epsilon}{\partial\rho})\right] \quad (1)$$

For the single phase, the first term, called Coulomb force, is a predominant mechanism for EHD. When a high-voltage electric field is applied between a wire or a needle electrode and a plan electrode, ions appear. Interaction between free charge particles and the electric field leads to Colomb force. This secondary flow is important for a low Re number because the momentum flux of the secondary flow is small in comparison to the main flow.

Mechanism of charge injection

The EHD mechanism used in this study included a wire electrode as an injector and a plan electrode, covered the cylinder surface, as a collector. By the application of a high-voltage electric field between the wire and the plan, free charge particles formed around the wire and moved to the plan.

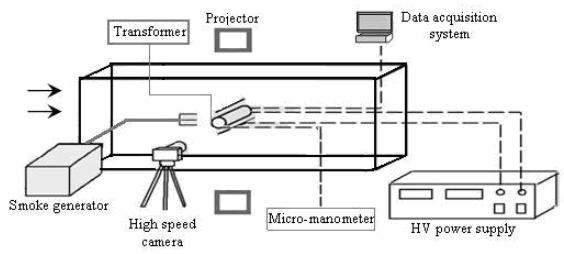

(a)

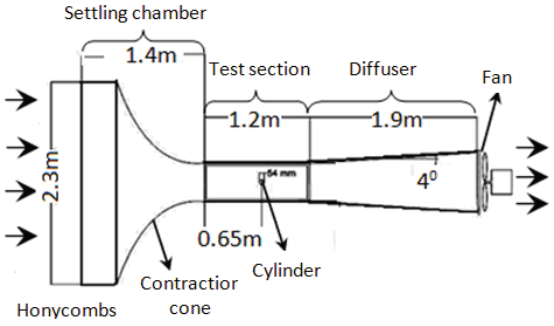

(b)

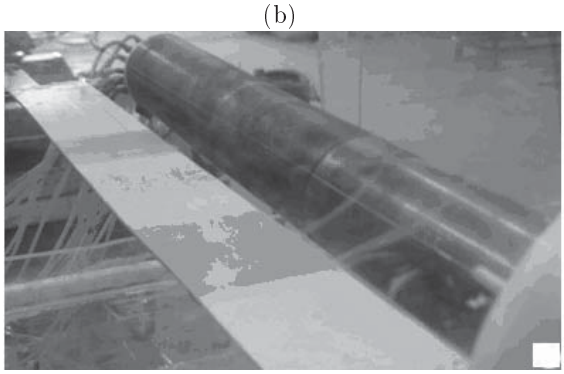

(c)

Figure 1. Experimental setup.

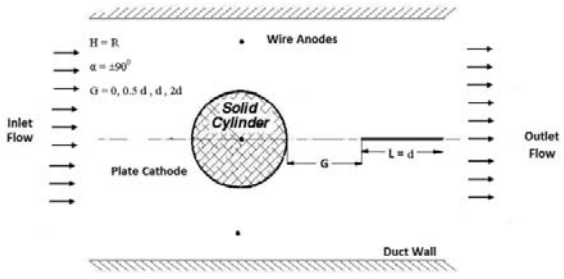

Figure 2. Arrangement of electrodes.

EXPERIMENTS

Wind–tunnel

Experiments were carried out in an open-circuit subsonic wind tunnel shown in Figures 1a, b, c. The settling chamber contains a honeycomb and then a 4.9 to 1 contraction cone. The contraction cone leads to the test section, which is a rectangular 0.43×0.43m duct with a length of metric converter ProductID1.28 m1.28 m. The walls of the channel are made of 5-mm-thick Plexiglas. The mainstream flow is generated by a variable speed axial fan at the end of the diffuser. The fan is driven by 7kW motor with a maximum speed of 3000 rpm. Two mainstream speeds of 1m/s and 2m/s are studied. Free stream turbulence is 0.5%. Figures 1a, b, c shows the wind tunnel and the schematic diagram of the experimental set up. The surrounding temperature is 30°C and Pr=0.708, k= 0.02624 W/m c, ρ= 1.1774 Kg/m^3 and μ= 1.8462× 10 $^{-5}$Kg/m s.

Cylinder and wires configurations

A smooth circular copper cylinder with an outer diameter D=5.4 cm, inner diameter D=5.0 cm and length L=44 cm was positioned horizontally, spanning the axis normal to the flow. The Copper wires with a diameter d=1 mm were used as positive discharge electrodes that were located symmetrically and parallel to the axis of the cylinder with spacing H=R at α=±90^0(as shown in Figure 3a). The splitter plate was an 0.054m×0.44m aluminum plate with a thickness of t=3 mm and was placed behind the cylinder at G = 0, 0.5d, d, 2d as shown in Figure 2.

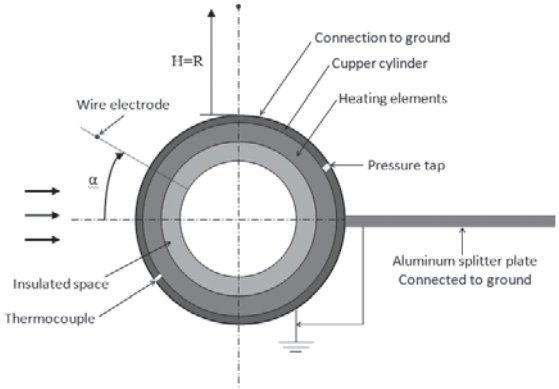

(a)

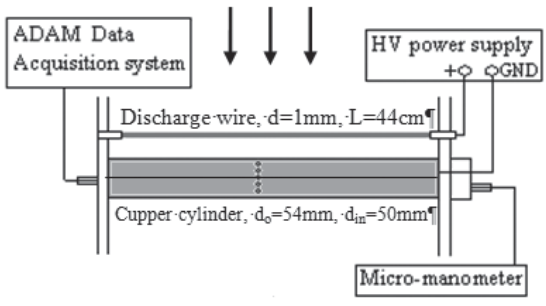

(b)

Figure 3. The schematic setup of electrodes, a) side view; b) top view

Surface thermal mapping by thermocouples and pressure measurements

The free stream air is maintained at the surrounding temperature level. The cylinder was heated by a 220Ω-heating element which produced a constant heat flux. To protect the pressure tubes and thermocouples, the space between the heater and pressure tubes and the thermocouples was insulated. 19 pressure tubes and 19 iron/Constantan (J type) thermocouples were embedded at 10° intervals on the cylinder. All measurements were done for the upper half of the cylinder because of the symmetry of geometry. The output of the thermocouples was fed to ADAM data acquisition system. The pressure tubes were connected to a set of micro manometers and then the pressure was measured. The side and top views of the cylinder are illustrated in Figures 3a, b. The side view has been enlarged.

Electrical properties of the DC corona discharge

The corona wind was produced by wire-plate actuators. The wires, as anode electrodes, were connected to a high-voltage (0-40kV) DC power supply with a positive polarity. The cylinder and the splitter plate were connected to the ground and used as cathode electrodes. Accuracy of the measured current and applied voltage are ± 2.5% and ± 2%, respectively.

Calculation of dimensionless variables

To explain heat transfer and hydrodynamic, we considered dimensionless variables such as C_p, C_d and Nu.

As mentioned before, 19 pressure tubes were located over the surface of the cylinder to measure P_i (static pressure).

Pressure force for i^{th} element would be:

$$F_i = P_i \Delta A_i, \quad \Delta A_i = rl\Delta\theta_i \tag{2}$$

where r and l are the cylinder radius and the length of cylinder, respectively. $\Delta\theta_i$ is the angle between i^{th} and $i+1^{th}$ pressure tubes that is 10^0 degree for all pressure tubes; therefore, ΔA_i equals 2.026×10^{-3} m^2. Drag is x-component of the pressure force:

$$D_i = F_i \cos\theta_i = P_i \cos\theta_i \Delta A_i \tag{3}$$

Total drag is:

$$D_p = \sum_{i=1}^{n} P_i \cos\theta_i \Delta A_i \tag{4}$$

For the drag over the cylinder, we just considered the variation of pressure drag, because friction drag is not notable. Friction drag for Re=3500 and 7000 are 7.82% and 5.66% of the total drag, respectively, as Khan *et.al.* (2004) explained analytically for elliptical cylinders.

A correlation based on Block Ratio (BR) correlation of Ota *et.al.* (1994) was performed for C_d.

$$C_d = C_d \left(1 - \frac{1}{8}BR\right) \tag{5}$$

h_i is local convection coefficient estimated as:

$$h_i = \frac{Q_{elect} - Q_{loss}}{\Delta A_i (T_i - T_\infty)} \tag{6}$$

where Q_{elect} is the electric power of the heater. T_i was measured by the thermocouples.

$$Q_{elect} = \frac{V^2}{R} = RI^2 \tag{7}$$

Resistance of the heater is R=220Ω and the applied voltage is V=54 V.

Energy balance for the cylinder is:

$$Q_{elect} = Q_{conv} + Q_{loss} \tag{8}$$

Q_{loss}, because of radiation and other losses, was estimated to be 10% of the total energy.

RESULTS AND DISCUSSION

For evaluation of the experiments, we compared the pressure coefficient of the present work with that of another work. The result of this comparison is shown in Figure 4.

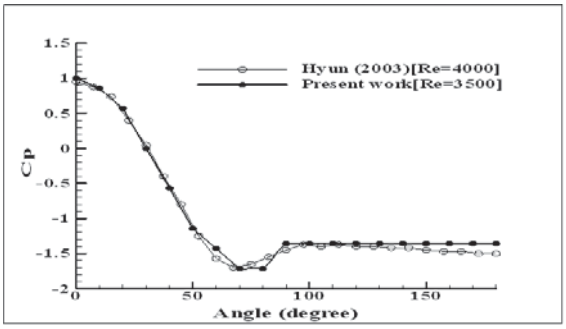

Figure 4. Comparison of the pressure coefficient.

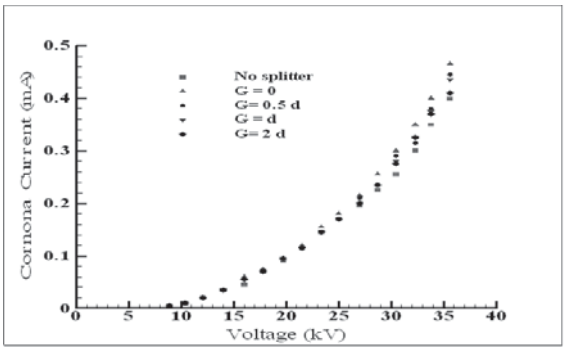

Figure 5. Corona current versus applied voltage.

Four corona discharge regimes appear by increasing applied voltage: spot type, glow regime, streamer and spark regime. Our experiments were performed in glow regime because this regime is suitable as a means of flow control (Hyun *et.al.* (2003)). Corona current versus applied voltage is shown in Figure 5. When H=R and a pair of wire electrodes were set at $\alpha=\pm 90°$, current-voltage curve is presented: (1) No splitter plate was placed behind the cylinder, (2) Splitter plate was at G=0, (3) Splitter plate was at G=0.5d, (4) Splitter plate was at G=d and (5) Splitter plate was at G=2d. By setting the splitter plate, corona current increased. When gap distance increased, corona current decreased

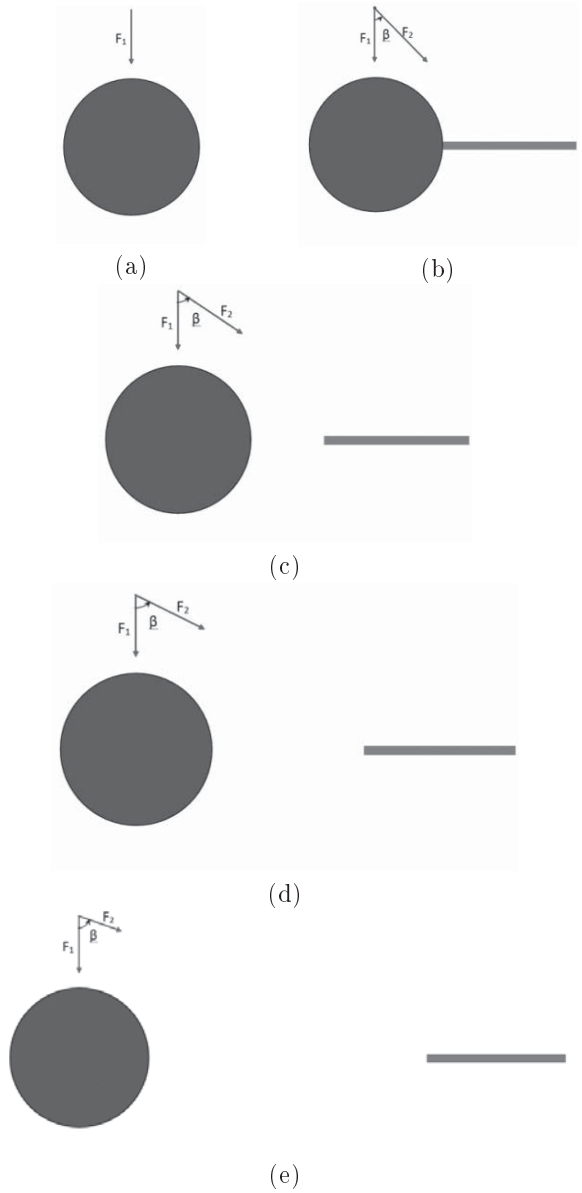

Figure 6. Schematic diagram of electric forces: a) No splitter plate, b) G=0, c) G=0.5d, d) G=d, e) G=2d.

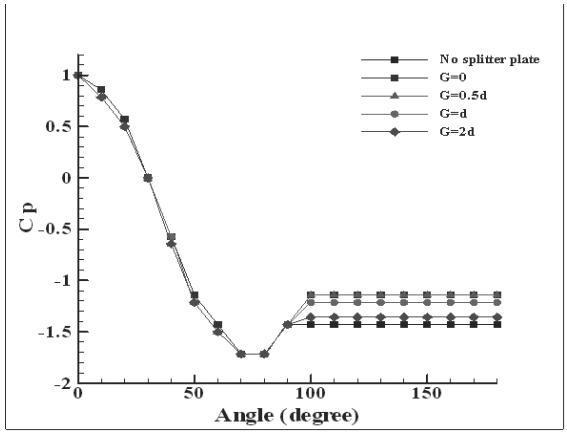

(a)

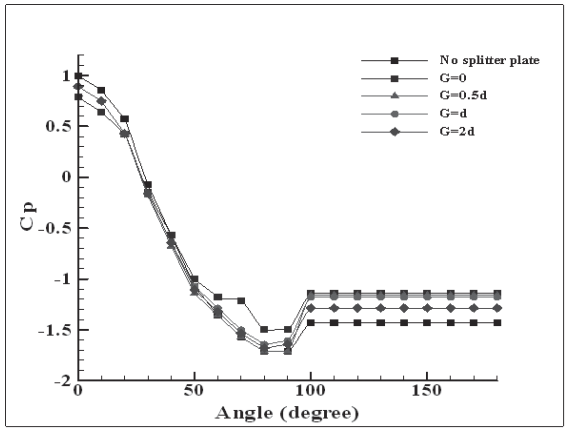

(b)

Figure 7. Pressure distribution over the cylinder surface, No EHD : a Re=3500.b Re=7000.

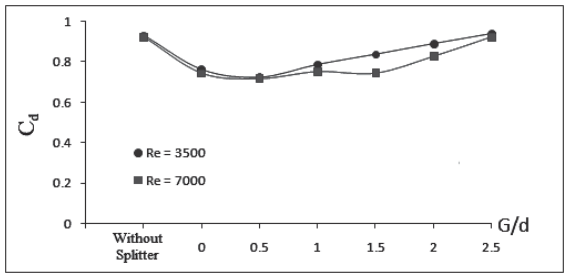

Figure 8. Pressure drag cofficient versus G/d,No EHD.

because of the reduction of the second corona wind effect.

Electrical forces for various locations of the splitter plate are shown schematically in Figure 6(a-e).

Experimental uncertainties were calculated based on the partial derivative method of Moffat (1988). The uncertainties for applied voltage, current and temperature were ±1%, ±2.5% and 1°C, respectively. We got a minimum value of 9% for Nu number as shown in Figure 21.

Figure 7a, b show the pressure coefficient C_p over

the cylinder for various locations of the splitter and two different Reynolds numbers, 3500 and 7000. As observed, the presence of the splitter plate behind the cylinder caused a dramatic increase in C_p. By increasing G, the effect of the splitter plate decreased. Generally, the splitter plate behind the cylinder suppresses vortex shedding and stabilizes it but when G =2d, this splitter plate doesn't play an important role. Fig 8 shows the drag coefficient for various G/d. When G=0, C_d decreased but by increasing G, it increased, too.

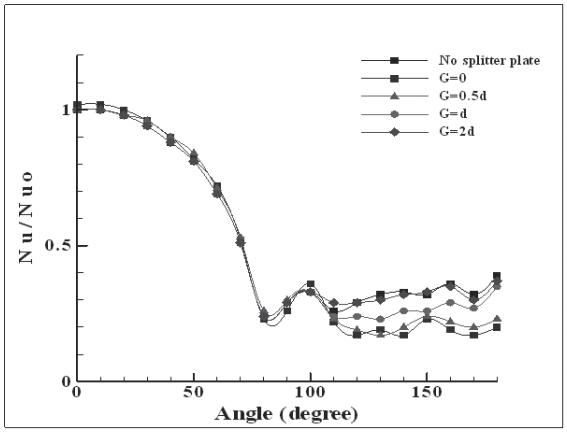

(a)

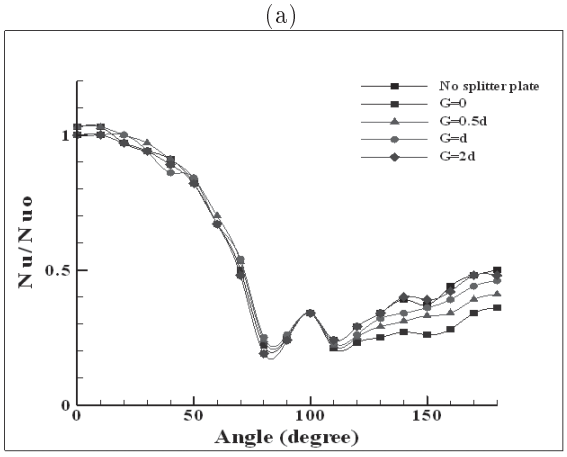

(b)

Figure 9. Relative local Nusselt number over the cylinder surface, No EHD, a) Re=3500. b) Re=7000.

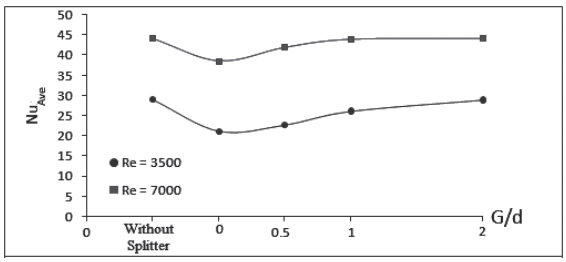

Figure 10. Average Nusselt number versus applied voltage, No EHD.

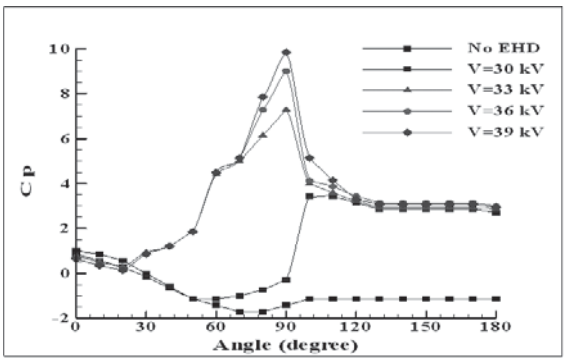

Figure 11. Pressure distribution over the cylinder surface, α=±90, G=0, Re=3500.

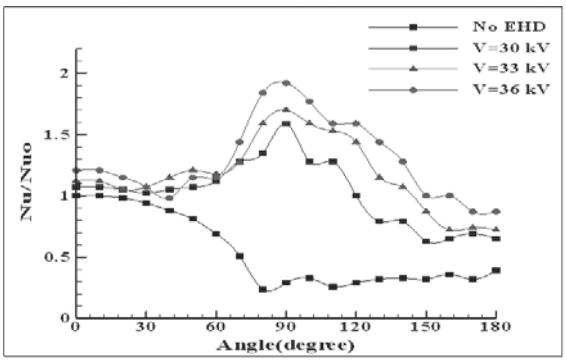

Figure 12. Relative local Nusselt number over the cylinder surface, α=±90, G=0, Re=3500.

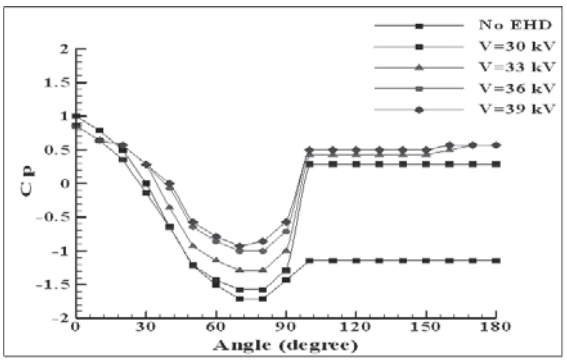

Figure 13. Pressure distribution over the cylinder surface, α=±90, G=0.5d, Re=3500.

Figure 9a, b illustrates the relative local Nusselt number over the cylinder for various gap distances at Re=3500, 7000, respectively. When the splitter plate is behind the cylinder, Nu/Nu_o decreased behind the cylinder but by increasing G, it increased, too. The average Nusselt number for various gap distances is illustrated in Figure 10.

When G=0, the pressure coefficient for various applied voltages is shown in Figure 11. Because of the notable effect of EHD actuation for low Reynolds numbers, the results were performed for Re=3500. C_p reached a maximum value at θ=90. External forces

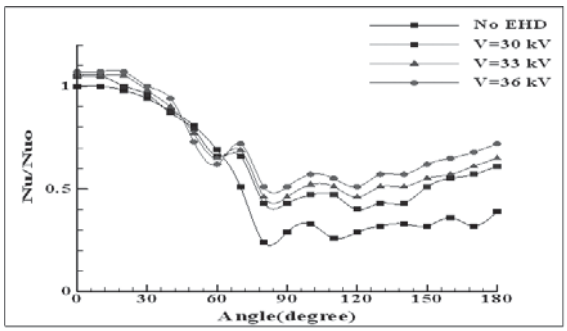

Figure 14. Relative local Nusselt number over the cylinder surface, α=±90,G=0.5d, Re=3500.

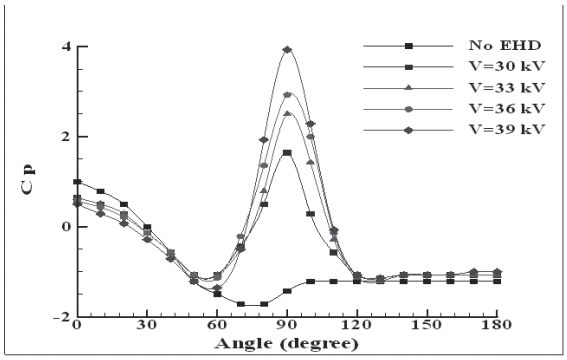

Figure 15. Pressure distribution over the cylinder surface, α=±90, G=d, Re=3500.

around the cylinder in this case (G=0) are shown schematically in Figure 6b. Two corona winds were recognized in the experiments: The first corona wind was between the wires and the cylinder and the second one was between the wires and the splitter plate. The first corona led to the formation of a recirculation zone before θ=90, which means that the pressure increased at θ=90 (Hyun *et.al.* (2003), Reza-zadeh *et.al.* (2010)). When applied voltage was increased, this corona wind got stronger and the maximum pressure increased. The second corona wind caused the movement of the flow toward the cylinder surface at $\theta > 90$ and the pressure increased behind the cylinder. The second corona made an angle (β) with normal direction as shown in Figure 6(b-e). Thus, the normal component ($F_2 \cos\beta$) made the first corona wind stronger. However, the horizontal component ($F_2 \sin\beta$) that was in the direction of the flow caused an increase in the component of x-velocity. In this case, β was small; thus, the normal component ($F_2 \cos\beta$) was greater than the horizontal component ($F_2 \sin\beta$). Figure 12 shows the relative local Nu number around the cylinder. By applying EHD actuation, because of the recirculation zone, heat transfer increased and Nu/Nu_o reached a maximum value at $\theta = 90$.

The pressure coefficient over the cylinder surface shown in Figure 13 displays the status of the splitter plate when it is placed at G=0.5d. A minimum value of C_p is observed before $\theta = 90$; then, C_p increased behind the cylinder. Electrical forces around the cylinder are illustrated schematically in Figure 6c. In this case, β is greater than the previous case (G=0); thus, the normal component $F_2 \cos\beta$ got smaller and the horizontal component $F_2 \sin\beta$ got greater. The effective corona wind ($F_1 + F_2 \cos\beta$) that caused the reattachment of the flow became weaker and $F_2 \sin\beta$ that led to the separation of the flow became greater; hence, the separation happened before $\theta = 90$. The relative local Nu number around the cylinder is shown in Figure 14. It reached a minimum value before $\theta = 90$ but because of the second corona wind, Nu/Nu_o increased behind the cylinder.

The pressure coefficient displayed in Figure 13 shows the status of the splitter plate when it is placed at G=D. The maximum value of C_p was at $\theta = 90$ but it did not increase considerably behind the cylinder. Figure 6d shows the schematic electrical forces. Because of the increment of gap distance, the effect of the second corona wind decreased; hence, its components got weaker and the reattachment happened at $\theta = 90$. The maximum C_p was at $\theta = 90$ but because of the second weak corona wind it did not increase considerably behind the cylinder. The relative local Nu number around the cylinder is shown in Figure 16.

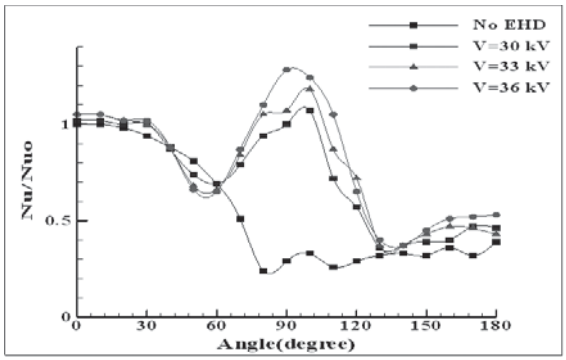

Figure 16. Relative local Nusselt number over the cylinder surface, α=±90, G=d, Re=3500.

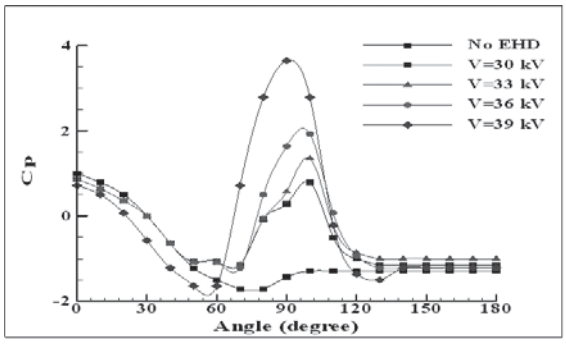

Figure 17. Pressure distribution over the cylinder surface, α=±90, G=2d, Re=3500.

The maximum value was about $\theta = 90$ because of the reattachment.

The coefficient shown in Figure 13 illustrates the status of the splitter plate when it is placed at G=2D. The maximum value of C_p was observed to be about $\theta = 90$. Electrical forces are shown schematically in Figure 6e. Because of the second weak corona wind, the effect of the splitter plate is not as considerable as the other cases. The relative local Nu number around the cylinder is shown in Figure 18. It reached a maximum value of about $\theta = 90$.

Figure 19 shows the drag coefficient for various locations of the splitter plate. When G=0, C_d was reduced dramatically and by increasing applied voltage, it increased, too. The average heat transfer coefficient is illustrated in Figure 20. As observed, in such conditions where there is no splitter plate, by increasing applied voltage, $\bar{N}u$ increased because the first corona wind got stronger. By applying the splitter plate, $\bar{N}u$ increased considerably. When the gap distance (G) increased, the effect of the splitter plate was reduced and $\bar{\nu}$ decreased.

CONCLUSION

A compound method (passive and active) was introduced to control the hydrodynamic behavior and heat transfer around a cylinder. The splitter plate, as a passive technique, and EHD actuators (wire-plate), as an active technique, were applied simultaneously. Experiments were performed for various locations of the splitter plate G=0, 0.5d, d, 2d when $\alpha=\pm 90°$, H=R at Re=3500, 7000. Two corona winds were recognized around the cylinder: the first corona wind was normal and the second one made an angle (β) with a normal direction. In the case G=0, a notable reduction of drag was obtained and heat transfer enhanced significantly. By increasing G, the second corona wind got weak and when G reached 2d, the effect of the splitter plate was not as considerable as the other cases. When G=0.5d, a new phenomenon was observed because of the interaction between the two corona winds. In this case, both of them are strong and can affect the flow.

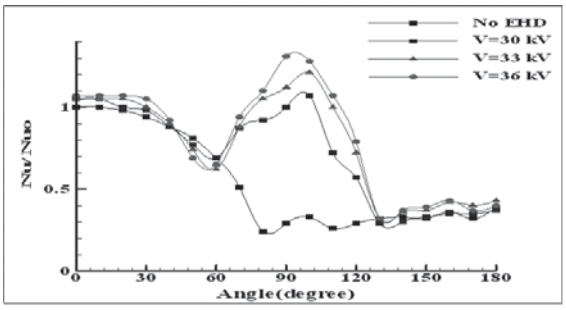

Figure 18. Relative local Nusselt number over the cylinder surface, $\alpha=\pm 90$,G=2d, Re=3500.

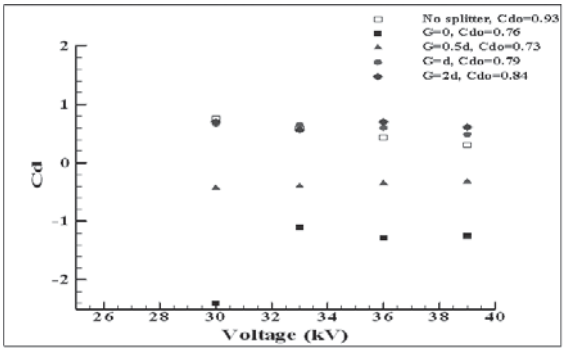

Figure 19. Pressure drag cofficient versus applied voltage, $\alpha=\pm 90$.

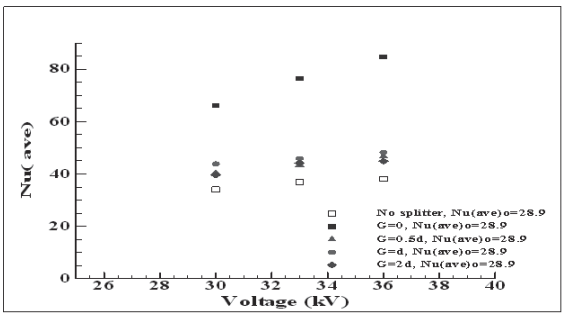

Figure 20. Average Nusselt number versus applied voltage, $\alpha=\pm 90$.

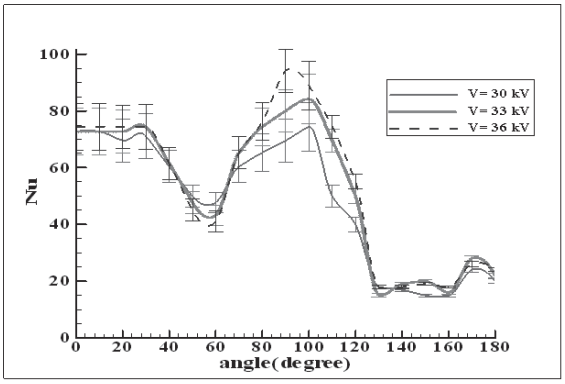

Figure 21. Analysis of uncertainities for relative local Nusselt number over the cylinder surface, $\alpha=\pm 90$, Re=3500.

REFERENCES

1. Artana, G., Sosa, R., Moreau, E., Touchard, G., "Control of the near-wake flow around a circular cylinder with electrohydrodynamic actuators", *Experiment in Fluids*, **36**, PP 580-588(2003).
2. Chang, J.S., Brocilo, D., Urashima, K., Dekowskib, J., Podlinskib, J., "On-set of EHD turbulence for cylinder in cross flow under corona discharges", *Journal of Electrostatics*, **64**, PP 569-573(2006).
3. Reza-zadeh, S., Masumi H., Esmaeilzadeh E., "Experimental study of heat transfer around cylinder in presence of electric field", *JAST*, **6(2)**, PP 87-97(2010).

4. Hauksbee, F., "Physico-mechanical experiments on various subjects", *London*, PP 46-47(1719).
5. Hwang, J.Y., Yang, K.S., Sun, S.H., "Reduction of flow-induced forces on circular cylinder using a detached splitter plate", *Physics of Fluids*, **15**(8), PP 2433-2436(2003).
6. Hwang J.Y., Yang K.S., "Drag reduction on a circular cylinder using dual detached splitter plates", *Journal of Wind Engineering and Industrial Aerodynamics*, **95**, PP 551-564(2007).
7. Hyun, K.T., Chun, C.H., "The wake flow control behind a circular cylinder using ion wind", *Experiments in Fluids*, **35**, PP 541-552(2003).
8. Jukes, T.N., Choi, K.S, "Flow control around a circular cylinder using pulsed dielectric barrier discharge surface plasma", *Physics of Fluids*, **21**, (2009).
9. Khan, W.A., Culham, J.R., Yovanovich, M.M., "Fluid flow and heat transfer from elliptical cylinders: analytical approach", *37th AIAA thermophysics conference, Portland, AIAA 2004-2272*, PP 1-11(2004).
10. Leger, L., Moreau, E., Artana, G., Touchard, G., "Influence of a DC corona discharge on the airflow along an inclined flat plate", *Journal of Electrostatics*, PP 300-306(2001).
11. Leger, L., Moreau, E., Gerard, G., Touchard, G., "Effect of a DC Corona Electrical Discharge on the Airflow along a Flat Plate", *IEEE Transactions on Industry Applications*, **38**, PP 1478-1485(2002).
12. Moffat, R.J., "Describing the uncertainties in experimental results", *Experimental Thermal and Fluid Science*, **1**, PP 3-17(1988).
13. Ota, T., Okamoto, Y., Yshikawa, H., "A correction formula for wall effects on unsteady forces of two-dimensional bluff bodies", *Journal of Fluids Engineering*, **12**, PP 414-418(1994).
14. Ozono, S., "Flow control of vortex shedding by a short splitter plate asymmetrically arranged downstream of a circular cylinder", *Physics of Fluids*, **11**, PP 2928-2934(1999).
15. Ozono, S., "Flow control of vortex shedding by asymmetrically arranged plates", *Theoretical and Applied Mechanics*, **49**, PP 191-196(2000).
16. Roshko, A., "On the drag and shedding frequency of two-dimensional bluff bodies", *National Advisory Committee for Aeronautics, Technical Note 3169*, PP 1-29(1954).
17. Shukla, S., Govardhan, R.N., Arakeri, J.H., "Flow over a cylinder with a hinged-splitter plate", *Journal of Fluids and Structures*, **25**, PP 713-720(2009).
18. Tiwari, S., Chakraborty, D., Biswas, G., Panigrahi, P.K., "Numerical prediction of flow and heat transfer in a channel in the presence of a built-in circular tube with and without an integral wake splitter", *International Journal of Heat and Mass Transfer*, **48**, PP 439-453(2005).